Sensitivity and Optimization of a High-Q Sapphire Dielectric Motion-Sensing Transducer

Brett D. Cuthbertson, Michael E. Tobar, *Member, IEEE*, Eugene N. Ivanov, and David G. Blair

***Abstract*—A high-Q sapphire dielectric motion sensing transducer that operates at microwave frequencies has been developed. The device uses cylindrical whispering gallery modes of quality factor greater than 10^5 at room temperature and greater than 10^8 at 4 K. The tuning coefficient of the transducer resonance frequency with respect to displacement was measured to be of the order of a few MHz/μm. An electromagnetic model that predicts the resonant frequency and tuning coefficient has been developed and was verified by experiment. We implemented the model to determine what aspect ratio and what dielectric mode is necessary to maximize the sensitivity. We found that the optimum mode type was a TM whispering gallery mode with azimuthal mode number of about 7 for a resonator of 3 cm in diameter. Also, we determined that the tuning coefficients were maximized by choosing an aspect ratio that has a large diameter with respect to the height. By implementing a microwave pump oscillator of SSB phase noise −125 dBc/Hz at 1 kHz offset, we have measured a sensitivity of order 10^{-16} m/$\sqrt{\text{Hz}}$. We show that this can be improved with existing technology to 10^{-18} m/$\sqrt{\text{Hz}}$, and that in the near future this may be further improved to 10^{-19} m/$\sqrt{\text{Hz}}$.**

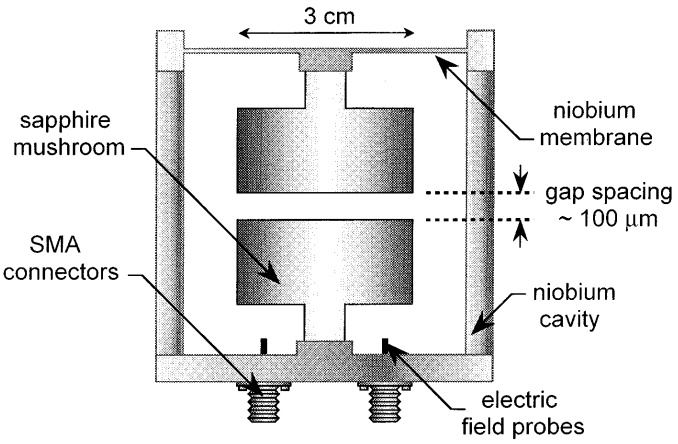

Fig. 1. The sapphire transducer, showing the two sapphire dielectric cylinders or mushrooms contained within a superconducting niobium shield to eliminate radiation loss. Two electric field probes are used to couple to and from the cavity, both are set for near unity electrical coupling at a temperature of 4.2 K. The transducer can be operated in both reflection and transmission. A gap spacing of ∼100 μm is used to ensure a high tuning coefficient as well as easy construction.

I. Introduction

Parametric transducers consisting of a displacement sensitive electromagnetic resonant cavity driven by a RF field, have been under development as ultrasensitive motion sensors since the 1980s [1]–[5]. For high sensitivity, the resonant cavity must have a high quality factor and frequency-displacement tuning coefficient. Also, the cavity must be driven with a low noise RF oscillator, and the modulated signal must be read out with a low noise RF amplifier.

During the 1980s the most sensitive parametric transducers were superconducting devices developed for operation at liquid helium temperatures. This research was driven by the need for ultra-low noise motion sensors to read out the effect of a gravitational wave changing the state of vibration of massive 1 ton acoustic resonator. During the early 1990s the technology was proven experimentally [6] with the niobium re-entrant cavities in use at the University of Western Australia. An alternative technology uses inductive or capacitive transducers that rely on low noise amplification using SQUID amplifiers [7]. Both these techniques have achieved a sensitivity of order 10^{-17} m/$\sqrt{\text{Hz}}$ to date. However, in principle the parametric transducer can outperform those based on SQUID amplifiers, and has the potential to measure below the zero point quantum mechanical fluctuations of the mechanical motion [8], [9].

More recently low loss dielectric materials such as sapphire have been used to construct high-Q parametric transducers that even perform well at room temperatures as well as cryogenic temperatures [9]–[12]. A schematic of the sapphire transducer is shown in Fig. 1. The dielectric cavity consists of a niobium cavity with a sapphire dielectric disk fixed rigidly to the bottom end plate of the cavity. A second dielectric disk was held directly above the first with a gap spacing of the order of 100 μm. The second disk was glued to a niobium membrane that had an acoustic resonant frequency of 1 kHz when it was loaded with the sapphire mass. Thus the motion of the acoustic membrane was sensed by the change in the electrical resonant frequency of the sapphire dielectric due to the change in gap spacing. The electromagnetic resonance was pumped by a microwave oscillator which was in turn modulated by

Manuscript received September 8, 1997; accepted January 6, 1998. This research was supported by the Australian Research Council and the University of Western Australia.

B. D. Cuthbertson, M. E. Tobar, E. N. Ivanov, and D. G. Blair are with the Department of Physics, University of Western Australia, Nedlands 6907, Western Australia, Australia (e-mail: mike@pd.uwa.edu.au).

the motion of the niobium membrane changing the gap spacing.

This effect has been applied to another example known to the frequency control community [13], and includes mode calculations comparable to those presented here. This work used the tuning due to thermal contraction of the gap spacing to compensate the frequency-temperature dependence of permittivity of the double disk sapphire resonator. The most sensitive dielectric resonances are the higher order Whispering Gallery (WG) modes. They exhibit high electrical quality factors and relatively high tuning coefficients of order MHz/μm.

The modelling of the dielectric resonator presented in Section II focuses on the use of WG modes. Once the model has been established, we utilize it to optimize the sensitivity of the dielectric transducer. Following this we experimentally determine the displacement sensitivity of the sapphire transducer and calculate what may be achievable in the near future if we use a new generation of ultra-low noise microwave oscillators [14], [15] to drive the sapphire transducer.

II. The Electromagnetic Model

We have developed an approximate electromagnetic model for a double disk dielectric transducer that predicts the frequency and tuning coefficient. Such models have already been developed by Tobar and Mann [16] to calculate the resonant frequencies in a sapphire dielectric resonator, and Peng Hong [17] to calculate the resonant frequencies and tuning coefficients in a room temperature sapphire transducer. These models were originally based upon the mode matching technique presented in Kajfez and Guillon [18] (and references therein). The aim of the modelling was to enable reliable prediction of the tuning coefficients for any given gap spacing, and possibly suggest a geometry that would enhance the tuning coefficient. It was also an aim to investigate if the tuning coefficient could be optimized by an appropriate choice of azimuthal mode number.

The mushroom-shaped sapphire elements (hereafter referred to as the dielectric system) can be modelled using the solutions obtained from Maxwell's equations solved in a cylindrical coordinate system (r, ϕ, z) for an anisotropic cylindrically symmetric dielectric material. The solutions for this system have been derived previously by Tobar and Mann [16] and is an extension to the solutions presented in Kajfez and Guillon [18]. The dielectric system can be divided into four regions. The system possesses both axial and cylindrical symmetry and this allows us to consider only the one quadrant in Fig. 2 when matching the fields on the boundary interface between the dielectric and free space. However, the gain in this simplicity is at the expense of obtaining only approximate solutions to Maxwell's equations as some less significant spatial regions are ignored in this paper. The free space regions adjacent to regions 2 and 3, and adjacent to regions 2 and 4 are ignored, as well as the neglect of the dielectric region comprising the support structure of the disk. Later it is shown that for our modes of interest only a 0.5% error is obtained using this approximation.

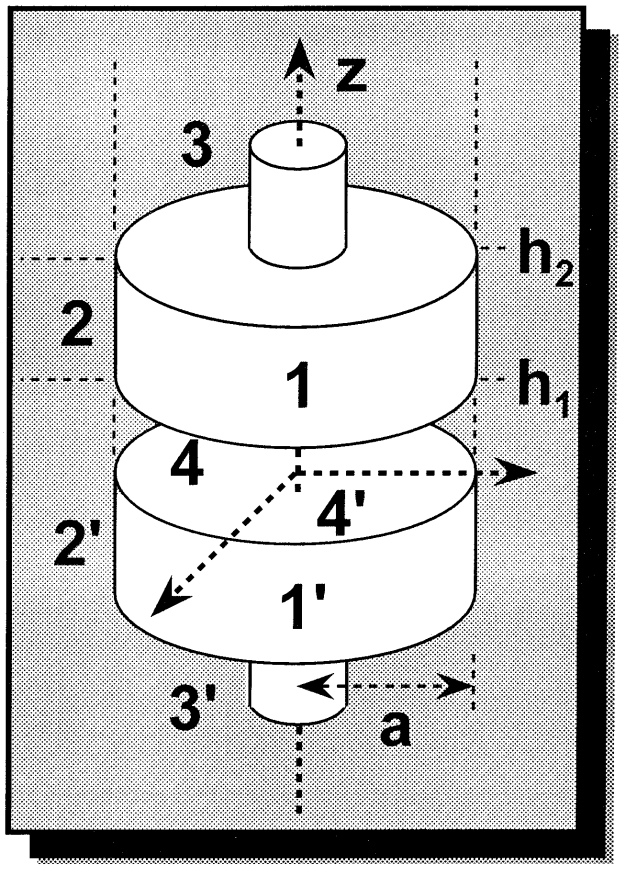

Fig. 2. The dielectric system, showing the regions used in the mode matching method to calculate the resonant frequencies. The two mushrooms have been distinguished by the use of primes on the region labels. The axial and cylindrical symmetry allows us to consider only the upper left quadrant in the model. Note that two regions have not been included in the model, implying that the model cannot be applied to modes in which a significant amount of field penetrates into these neglected regions.

Sapphire has an anisotropic dielectric permittivity, and to keep the fields symmetrical the axial direction has been chosen to be aligned with the crystallographic c-axis. The permittivity along the axial direction is defined as ε_z, while the permittivity in the azimuthal and radial coordinate is $\varepsilon_r (\varepsilon_r = \varepsilon_\phi)$. For completeness, it is also assumed that the permittivity outside the dielectric is that of free space and thus $\varepsilon_{\text{out}} = 1$.

Approximate electric field solutions in their respective regions can be found using the separation of variables tech-

nique and are of the form:

$$\begin{aligned} E_{z1} &= A_E J_m[k_E r]\cos[m\phi](A_1 \sin\beta z + B_1 \cos\beta z) \\ E_{z2} &= B_E K_m[k_{\text{out}} r]\cos[m\phi](A_1 \sin\beta z + B_1 \cos\beta z) \\ E_{z3} &= C_E J_m[k_E r]\cos[m\phi] e^{-\alpha_E z} \\ E_{z4} &= D_E J_m[k_E r]\cos[m\phi] \begin{cases} \cosh[\alpha_E z] \\ \sinh[\alpha_E z] \end{cases} \end{aligned} \tag{1}$$

where the J_m are Bessel functions of the first kind, and the K_m are modified Bessel functions of the second kind. A_E, B_E, C_E, D_E, A_1, and B_1 are amplitudes yet to be determined.

Likewise, the magnetic field solutions in their respective regions are:

$$\begin{aligned} H_{z1} &= A_H J_m[k_H r]\sin[m\phi](A_1 \sin\beta z + B_2 \cos\beta z) \\ H_{z2} &= B_H K_m[k_{\text{out}} r]\sin[m\phi](A_1 \sin\beta z + B_2 \cos\beta z) \\ H_{z3} &= C_H J_m[k_H r]\sin[m\phi] e^{-\alpha_H z} \\ H_{z4} &= D_H J_m[k_H r]\sin[m\phi] \begin{cases} \cosh[\alpha_H z] \\ \sinh[\alpha_H z] \end{cases} \end{aligned} \tag{2}$$

where

$$k_E^2 = \varepsilon_z k_o^2 - \frac{\varepsilon_z}{\varepsilon_r}\beta^2 \quad k_H^2 = \varepsilon_r k_o^2 - \beta^2 \quad k_{\text{out}}^2 = \varepsilon_{\text{out}}\beta^2 - k_o^2 \tag{3}$$

$$\alpha_E^2 = (\varepsilon_z - 1)k_o^2 - \frac{\varepsilon_z}{\varepsilon_r}\beta^2 \quad \alpha_H^2 = (\varepsilon_r - 1)k_o^2 - \beta^2. \tag{4}$$

Several parameters have been introduced in (2), (3), and (4): m is the azimuthal mode number (i.e., the number of standing waves in the azimuthal direction), and β is the axial propagation constant that determines the axial order of the mode. The radial propagation constant k_{out} determines the distance the mode penetrates into the region outside the dielectric. Similarly, k_E and k_H are the radial propagation constants for the electric and magnetic fields, respectively, inside the dielectric. Outside the dielectric α_E and α_H are the axial propagation constants for the electric and magnetic fields, respectively. These determine the penetration of the fields in the axial directions.

Only the axial solutions are required directly from Maxwell's equations, as the remaining transverse solutions can be obtained through the following relations:

$$\begin{aligned} H_\phi &= \frac{1}{k_i^2}\left(-j\omega\varepsilon_o\varepsilon_i\frac{\partial E_z}{\partial r} + \frac{1}{r}\frac{\partial^2 H_z}{\partial z \partial \phi}\right) \\ E_\phi &= \frac{1}{k_i^2}\left(-j\omega\mu\frac{\partial H_z}{\partial r} + \frac{1}{r}\frac{\partial^2 E_z}{\partial z \partial \phi}\right) \\ H_r &= \frac{1}{k_i^2}\left(j\omega\varepsilon_o\varepsilon_i\frac{1}{r}\frac{\partial E_z}{\partial \phi} + \frac{\partial^2 H_z}{\partial z \partial r}\right) \\ E_r &= \frac{1}{k_i^2}\left(-j\omega\mu\frac{1}{r}\frac{\partial H_z}{\partial \phi} + \frac{\partial^2 E_z}{\partial z \partial r}\right). \end{aligned} \tag{5}$$

Here $k_i = k_H$ in regions 1, 3, and 4 and $k_i = k_{\text{out}}$ in region 2, and $\varepsilon_i = \varepsilon_r$ in region 1, and $\varepsilon_i = 1$ (or ε_{out} if the region outside the dielectric is not free space) in regions 2, 3, and 4. Having found approximate solutions to Maxwell's equations, we use the boundary conditions to find the particular solution for the given geometry. Once again, the axial and cylindrical symmetry of the dielectric system enables us to constrain the radial coordinate independently of the axial coordinate.

To obtain the radial match condition, we impose the continuity of the tangential components of the electric and magnetic fields at the boundary $r = a$ (the radius of the mushroom). These conditions are:

$$\begin{aligned} E_{z1} = E_{z2} \quad H_{z1} = H_{z2} \\ E_{\phi 1} = E_{\phi 2} \quad H_{\phi 1} = H_{\phi 2} \end{aligned} \tag{6}$$

After making the substitutions, we obtain four equations

$$\begin{aligned} A_E J_m[k_E a] - B_E K_m[k_{\text{out}} a] &= 0 \\ A_H J_m[k_H a] - B_H K_m[k_{\text{out}} a] &= 0 \\ -A_E\frac{m\beta}{k_H^2 r}J_m[k_E a] + B_E\frac{m\beta}{k_{\text{out}}^2 r}K_m[k_{\text{out}} a] & \\ -A_H\frac{\mu\omega}{k_H}J'_m[k_H a] + B_H\frac{\mu\omega}{k_{\text{out}}}K'_m[k_{\text{out}} a] &= 0 \\ -A_H\frac{m\beta}{k_H^2 r}J_m[k_H a] + B_H\frac{m\beta}{k_{\text{out}}^2 r}K_m[k_{\text{out}} a] & \\ -A_E\frac{\varepsilon_o\varepsilon_r k_E\omega}{k_H^2}J'_m[k_E a] + B_E\frac{\varepsilon_o\varepsilon_{\text{out}}\omega}{k_{\text{out}}}K'_m[k_{\text{out}} a] &= 0. \end{aligned} \tag{7}$$

We can simplify these equations further by introducing new variables (x_E, x_H, y) scaled to the radius of the mushrooms, where:

$$x_E = k_E a \qquad x_H = k_H a \qquad y = k_{\text{out}} a. \tag{8}$$

Equations (7) in the new coordinates become:

$$\begin{aligned} A_E J_m[x_E] - B_E K_m[y] &= 0 \\ A_H J_m[x_H] - B_H K_m[y] &= 0 \\ -A_E\frac{m\beta}{x_H^2}J_m[x_E] + B_E\frac{m\beta}{y^2}K_m[y] & \\ -A_H\frac{\mu\omega}{x_H}J'_m[x_H] + B_H\frac{\mu\omega}{y}K'_m[y] &= 0 \\ -A_H\frac{m\beta}{x_H^2}J_m[x_H] + B_H\frac{m\beta}{y^2}K_m[y] & \\ -A_E\varepsilon_o\varepsilon_r\omega\frac{x_E}{x_H^2}J'_m[x_E] + B_E\frac{\varepsilon_o\varepsilon_{\text{out}}\omega}{y}K'_m[y] &= 0. \end{aligned} \tag{9}$$

We can write these equations in matrix form, so:

$$\mathbf{F}|U\rangle = 0 \tag{10}$$

where $|U\rangle = [A_e, A_H, B_E, B_H]$ and the matrix $\mathbf{F}$ is given by:

$$\mathbf{F} = \begin{bmatrix} J_m[x_E] & 0 & -K_m[y] & 0 \\ 0 & J_m[x_H] & 0 & -K_m[y] \\ -\frac{m\beta}{x_H^2}J_m[x_E] & \frac{\mu\omega}{x_H}J'^{m[x_H]} & -\frac{m\beta}{y^2}K_m[y] & \frac{\mu\omega}{y}K'_m[y] \\ \varepsilon_o\varepsilon_r\omega\frac{x_E}{x_H^2}J'_m[x_E] & -\frac{m\beta}{x_H^2}J_m[x_H] & \frac{\varepsilon_o\varepsilon_{\text{out}}\omega}{y}K'_m[y] & -\frac{m\beta}{y^2}K_m[y] \end{bmatrix}, \tag{11}$$

Equation (11) can only be satisfied if the determinant of the matrix $\mathbf{F}$ vanishes. Taking the determinant of $\mathbf{F}$ we obtain (where we set $\varepsilon_{\text{out}} = 1$):

$$\left(\varepsilon_r \frac{x_E}{x_H^2}\frac{J_m'[x_E]}{J_m[x_E]} + \frac{K_m'[y]}{yK_m[y]}\right)\left(\frac{J_m'[x_H]}{x_H J_m[x_H]} + \frac{K_m'[y]}{yK_m[y]}\right) - m^2\frac{(x_H^2+\varepsilon_r y^2)}{x_H^4 y^4}(x_H^2+y^2) = 0 \quad (12)$$

where we have used the substitutions:

$$\omega = k_o/\sqrt{\mu\varepsilon_o} \qquad \beta^2 = (x_H^2+\varepsilon_r y^2)/a^2(\varepsilon_r - 1)$$
$$k_o^2 = (x_H^2+y^2)/a^2(\varepsilon_r - 1). \quad (13)$$

We note that (12) is completely independent of the axial coordinate and, therefore, holds for any cylindrical dielectric slab of arbitrary height. Solving this equation independent of any axial match will give the resonant frequencies of an infinite cylindrical waveguide. Equation (12) also can be solved independently of any physical dimensions due to an appropriate transformation of the variables k_E, k_H, and k_{out} to x_E, x_H, and y, respectively.

In a similar fashion we can apply the boundary conditions (one at $z = h_2$ and the other at $z = h_1$) in the axial coordinate to obtain a second equation. However, we can simplify the axial analysis significantly if we assume the mode is quasi-TM (Transverse Magnetic, or $\mathbf{E_z}$) or quasi-TE (Transverse Electric, or $\mathbf{H_z}$). For TM mode solutions the axial component of the magnetic field is assumed to be zero, and for TE mode solutions the axial component of the electric field is assumed to be zero. The axial match could be done more accurately if we calculated the percentage of the $\mathbf{E_z}$ and $\mathbf{H_z}$ components and then matched both components simultaneously as we did for the radial match. However, this would unnecessarily add to the complication of the analysis as this approximation is already up to 0.5% accurate for calculating the frequency for WG modes, and even more accurate in calculating the relative frequency shift with displacement. The only reason to do a more complicated analysis would be if the frequency of the hybrid modes were needed more accurately than a few percent. Because these modes exhibit high radiation and loss, and thus low Q-factors, this is not necessary.

For TM mode solutions we take the field equations expressed in (1) and apply the following conditions;

$$H_{z1} = 0 \quad H_{z2} = 0$$
$$H_{z3} = 0 \quad H_{z4} = 0 \quad (14)$$

where we chose the hyperbolic cosine for modes with odd axial number ($p = 1, 3, 5, \ldots$), and the hyperbolic sine for modes with even axial number ($p = 0, 2, 4, \ldots$). In the past, several different designations have been used to denote a particular WG mode, in this discussion we shall choose the labels $TM_{m,n,p}$ and $TE_{m,n,p}$, where m is the azimuthal order, n is the radial order, and p is the axial order. The indices m, n, p describe the number of maxima in the field intensity along that particular coordinate within the dielectric. For example, the fundamental axial mode $TM_{8,1,1}$ ($m = 8$, $n = 1$, $p = 1$) describes 16 maxima in the azimuthal coordinate, a single maximum in the radial coordinate, and a single maximum in the axial coordinate. For the remainder of the analysis, we shall restrict ourselves to odd axial number modes; however, the same routine applies to modes with even axial numbers.

Imposing the continuity of the tangential field components along the boundary $z = h_2$ gives the following equations:

$$E_{r1} = E_{r3} \quad H_{r1} = H_{r3}$$
$$E_{\phi 1} = E_{\phi 3} \quad H_{\phi 1} = H_{\phi 3}. \quad (15)$$

After making the substitutions, we obtain four equations, of which two are independent:

$$C_E\alpha_E e^{-\alpha_E h_2} - A_E\beta(A_1\cos\beta h_2 - B_1\sin\beta h_2) = 0$$
$$C_E\varepsilon_{\text{out}}e^{-\alpha_E h_2} + A_E\varepsilon_r(A_1\sin\beta h_2 + B_1\cos\beta h_2) = 0. \quad (16)$$

Similarly at the boundary $z = h_1$ we obtain:

$$E_{r1} = E_{r4} \quad H_{r1} = H_{r4}$$
$$E_{\phi 1} = E_{\phi 4} \quad H_{\phi 1} = H_{\phi 4} \quad (17)$$
$$D_E\alpha_E\sinh\alpha_E h_1 + A_E\beta(A_1\cos\beta h_1 - B_1\sin\beta h_1) = 0$$
$$D_E\varepsilon_{\text{out}}\cosh\alpha_E h_1 + A_E\varepsilon_r(A_1\sin\beta h_1 + B_1\cos\beta h_1) = 0. \quad (18)$$

Writing the equations in matrix form, we can obtain the matrix equation similar to (10); however, the amplitude coefficient vector $\mathbf{U}$ is given by:

$$|U\rangle = [A_E A_1, C_E, A_E B_1, D_E]$$

and the matrix $\mathbf{F}$ is given by:

$$\mathbf{F} = \begin{bmatrix} -\beta\cos\beta h_2 & \alpha_E e^{-\alpha_E h_2} & \beta\sin\beta h_2 & 0 \\ \varepsilon_r\sin\beta h_2 & \varepsilon_{\text{out}}e^{-\alpha_E h_2} & \varepsilon_r\cos\beta h_2 & 0 \\ \beta\cos\beta h_1 & 0 & -\beta\sin\beta h_1 & \alpha_E\sinh\alpha_E h_1 \\ \varepsilon_r\sin\beta h_1 & 0 & \varepsilon_r\cos\beta h_1 & \varepsilon_{\text{out}}\cosh\alpha_E h_1 \end{bmatrix}. \quad (19)$$

Taking the determinant of the matrix $\mathbf{F}$ and setting $\varepsilon_{\text{out}} = 1$, we obtain the characteristic equation:

$$-\alpha_E\beta\varepsilon_r\cosh[\alpha_E h_1](\cos\beta h_1\cos\beta h_2 + \sin\beta h_1\sin\beta h_2) +$$
$$\beta^2\cosh[\alpha_E h_1](\cos\beta h_1\sin\beta h_2 - \cos\beta h_2\sin\beta h_1) -$$
$$\alpha_E\beta\varepsilon_r\sinh[\alpha_E h_1](\cos\beta h_1\cos\beta h_2 + \sin\beta h_1\sin\beta h_2) +$$
$$\alpha_E^2\varepsilon_r^2\sinh[\alpha_E h_1](\cos\beta h_2\sin\beta h_1 - \cos\beta h_1\sin\beta h_2) = 0. \quad (20)$$

Note that the axial equation above is not independent of the radial coordinate and depends on the radius of the dielectric system through the α_E and β propagation constants.

The roots of the two characteristic equations can be found numerically using a package such as Mathematica®

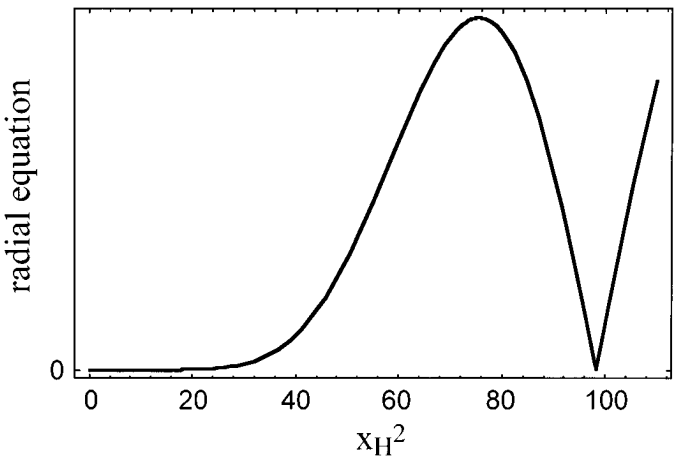

Fig. 3. The roots of the radial equation are found by plotting along a line of constant y^2. The roots of this equation are not a strong function of y^2 and so an arbitrary value of y^2 can be chosen as an initial starting point, say $y^2 = 5$. In this graph, the $TM_{8,1,1}$ ($m = 8$) mode radial equation has been plotted.

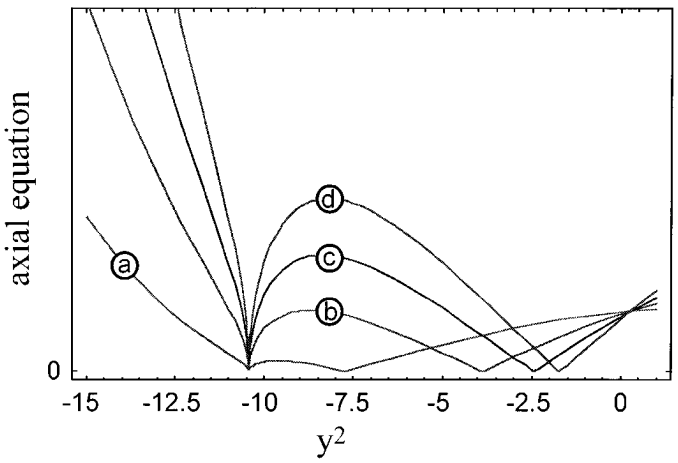

Fig. 4. The roots of the axial equation for several gap spacing values have been plotted above. Curve (a) shows the axial equation for a gap spacing of 50 μm, curve (b) at a gap spacing of 100 μm, curve (c) at a gap spacing of 150 μm, and curve (d) at 200 μm. The roots are found by plotting along a line of constant x_H^2. In this case caution needs to be taken to avoid the spurious root at $y^2 = -10.1$, which does not vary as a function of the gap spacing, thus $df/dx = 0$ for this root.

(Wolfram Research, Champaign, IL). Caution is required when numerically solving these equations for the first time. Blindly using a numerical solver will often return a spurious root, particularly for low values of x_H^2 where the equations are no longer valid (this region is characterized by a significant evanescent field in the regions ignored in the model). It is wise to approach the problem by first plotting the radial equation along some arbitrary y^2 value as in Fig. 3, and determining the value of x_H^2 that satisfies that equation. The mode frequency is a stronger function of the x_H^2 coordinate (and hence the radial coordinate) than y^2 (or axial coordinate) so, having determined a rough value of x_H^2, the calculated frequency can be checked with the expected frequency. After x_H^2 has been determined, the axial equation can be plotted as a function of the constant y^2 value as shown in Fig. 4.

Having graphically determined rough estimates of x_H^2 and y^2, it is possible to use a suitable numerical procedure to simultaneously find the roots $\{x_H^2, y^2\}$ as a function of the gap spacing. The resonant frequency then can be calculated as a function of the gap spacing, and hence the tuning coefficient df/dx can be calculated. As long as the starting estimates are close to the local root that corresponds to the solution, the result is independent of the starting guess as expected.

Errors in mode frequency calculations are consistent and comparable with previous analysis using a similar technique for a single sapphire resonator [16], [19]. For modes with $p = 0$ errors are less than .1% which is smaller than estimated uncertainties in permittivities and dimensions. Above $p = 2$ errors can be of the order -1% in TE modes and $+2\%$ in TM modes.

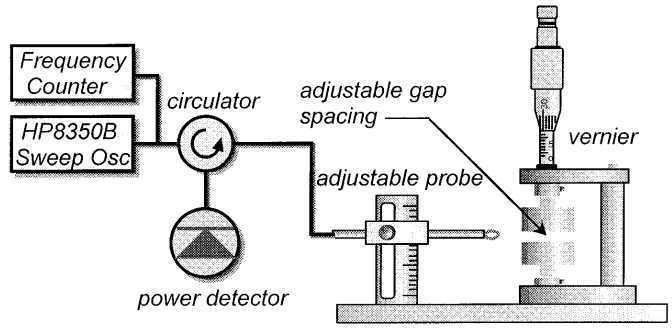

Fig. 5. The experimental technique used to measure the WG mode tuning coefficients. The frequency range of the HP8350B was 8.0 GHz to 13.0 GHz. By adjusting the height, distance, and azimuth relative to the sapphire mushrooms, it was possible to identify the correct WG mode and provide suitable coupling. The gap spacing between the sapphire mushrooms could be controlled and measured using the vernier scale with 1 μm resolution. The sapphire mushrooms themselves were placed in brass "nests" and locked in place using three screws. Slight nonparallel alignment was unavoidable in the experiment, and the effect of this can be seen in the results.

III. Verification with Experiment

The model originally was intended to predict, with sufficient accuracy, the tuning coefficients of the transducer for different azimuthal mode numbers. In this regard it has been highly successful, at least for the WG modes $TM_{7,1,1}$, $TM_{8,1,1}$, $TM_{9,1,1}$, $TM_{10,1,1}$ where we were able to compare the model results with the experimental data. However, the model also allows us to examine other aspects of the transducer's electromagnetic characteristics. The technique of measuring these modes experimentally is shown in Fig. 5.

Figs. 6 and 7 show the model results for the $TM_{7,1,1}$ mode, compared to those obtained through experiment. Fig. 6 shows the resonant frequency and Fig. 7 shows the

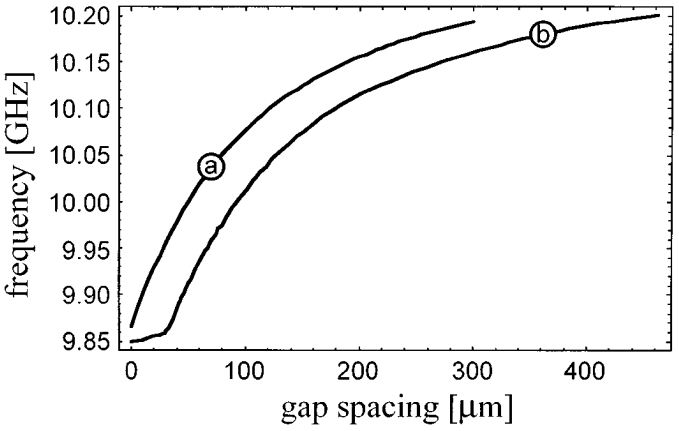

Fig. 6. The $TM_{7,1,1}$ mode frequency as a function of gap spacing. Curve (a) shows the theoretical curve determined from the model. Curve (b) shows the experimental results. For small gap spacings, the experimental results suggest that the tuning coefficient is low. This was a result of the imperfect alignment of the two sapphire mushrooms, resulting in the mushrooms touching at small gap spacings.

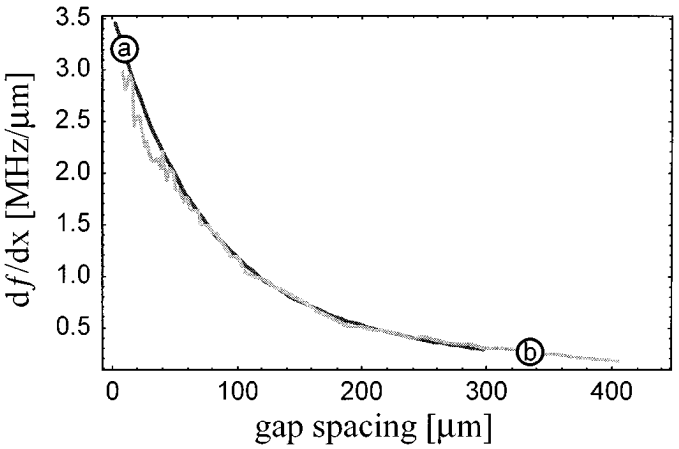

Fig. 7. The tuning coefficient df/dx as a function of gap spacing. Curve (a) shows the theoretical result. Curve (b) shows the experimental results. The theoretical and experimental tuning coefficients were calculated via numerical differentiation of the frequency data shown in Fig. 6.

tuning coefficient, as the distance between the sapphire mushrooms is increased. The change in resonant frequency with position can be measured and calculated more accurately than the absolute frequency. This is highlighted by the excellent agreement in tuning coefficient in Fig. 7 as compared to the absolute values in Fig. 6. When calculating the absolute frequency of WG modes, the uncertainty in the dimensions and positions of the sapphire mushrooms and the dielectric permittivities are the dominant sources of error. This is because the majority of the field is only present at the circumference of the cylinder with an almost TM or TE field structure. For hybrid modes the model itself becomes the dominant source of inaccuracy due to the approximations made from the axial match and the fact that more field is present in the ignored regions.

Similar results were obtained for the $TM_{8,1,1}$, $TM_{9,1,1}$, and $TM_{10,1,1}$ modes. The agreement between the model and experimental tuning coefficients was excellent.

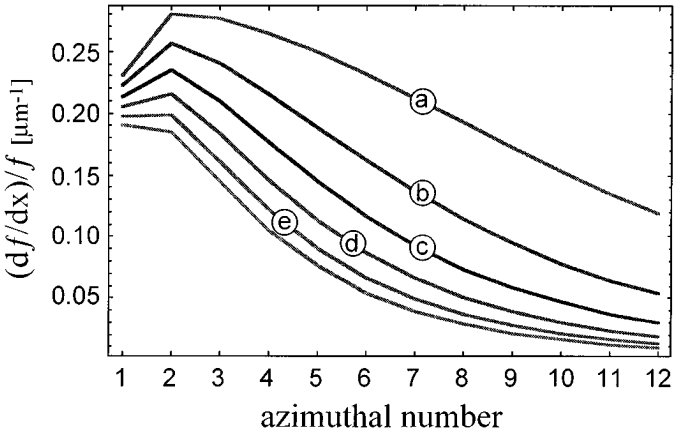

Fig. 8. The normalized tuning coefficient $(df/dx)/f$ as a function of azimuthal mode number for gap spacings of (a) 50 μm, (b) 100 μm, (c) 150 μm, (d) 200 μm, (e) 250 μm, and (f) 300 μm. The sensitivity of the transducer is not solely a function of the tuning coefficient and actually goes as $(df/dx)/f$. Therefore, the plots suggest that the optimum azimuthal mode number is 2.

IV. Optimization of the Tuning Coefficient

A. Effect of Azimuthal Mode Number and Gap Spacing

It was anticipated that an optimization could be made with respect to azimuthal mode number to choose the best WG mode for the transducer. One might expect that higher azimuthal mode numbers will display an increasingly confined electromagnetic field within the sapphire dielectric and, thus, less field in the gap. Hence, changes in the gap spacing will have a weaker effect and the tuning coefficient will be smaller. Also, at lower mode numbers the field becomes increasingly dispersed throughout the dielectric, and so the field density within the gap reduces, also resulting in a smaller tuning coefficient. From the combination of these two effects, we expect that there is an optimum azimuthal mode number m to maximize the sensitivity of the transducer.

Although the observed trend highlighted the conditions required for high tuning coefficients and confirmed our intuitive expectations, it is the combination of the electrical quality factor, Q_e, resonant frequency, f_o, and tuning coefficient, df/dx, that determine the electro-mechanical coupling, β_o, and, hence, the sensitivity. Therefore, to achieve the optimum sensitivity we need to look at the product $\beta_o \propto \frac{Q_e}{f_o}\left(\frac{df}{dx}\right)$.

Fig. 8 shows the normalized tuning coefficient or $(df/dx)/f$ as a function of the azimuthal mode number. These results suggest that the optimum sensitivity would be achieved using a mode number of 2. However, low mode numbers also exhibit low quality factors. Measurements taken at room temperature show that the quality factor increases almost linearly with azimuthal mode number [17], and it would not be unreasonable to assume the same to

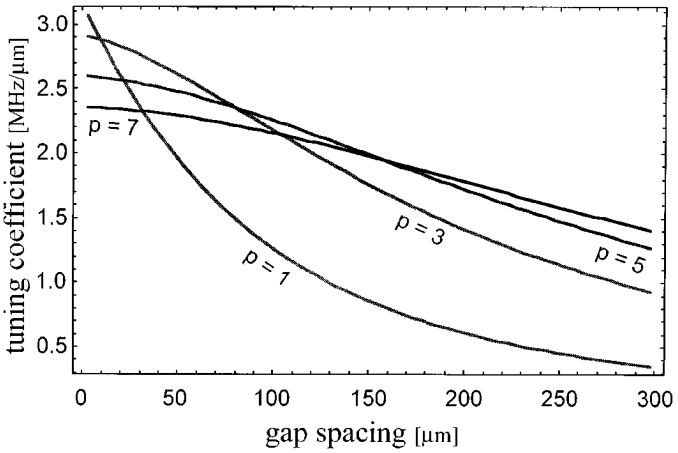

Fig. 9. The tuning coefficient as a function of gap spacing and axial mode number. The plots show that, as the axial order increases, the tuning coefficient remains high even for large gap spacings. However, experiments suggest that modes with high axial numbers are very difficult to detect and seem to be limited to a maximum axial number of three. Therefore, it is not practical to use these high axial order modes to maintain a high tuning coefficient over larger gap spacings.

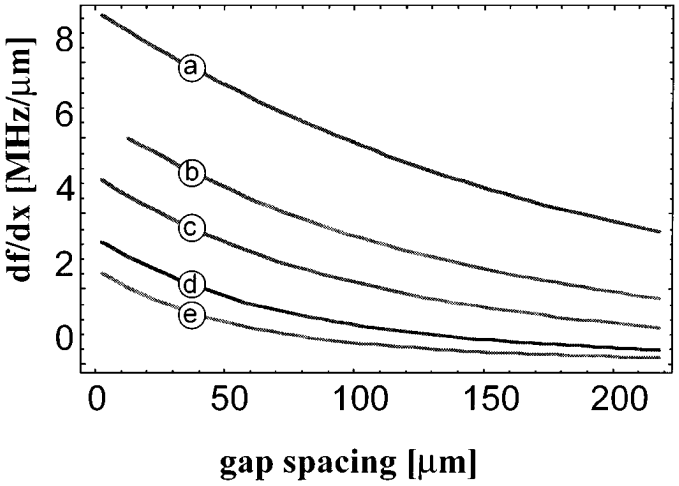

Fig. 10. The tuning coefficient of the $TM_{8,1,1}$ WG mode as a function of the gap spacing for several different height values in a cylinder with a diameter of 30 mm.

be true in a cryogenic system. An azimuthal mode number of about 7 would then be ideal.

We also examined the tuning coefficient as a function of the axial mode number. The results are summarized in Fig. 9, and they suggest that the higher the axial mode number the higher the tuning coefficient for larger gap spacings. In practice this is highly advantageous, as setting small gap spacings is difficult. Unfortunately modes with axial numbers greater than 2 are unstable and are not easily observed. This is because it is energetically more favorable to form a mode with a node in the gap rather than an antinode.

B. Dimension Optimization

We also were able to investigate how the tuning coefficient behaves for different cylinder heights. Previously, it was not known whether it would be possible to increase the tuning coefficient by fine-tuning the height-to-diameter ratio. We chose to examine the $E_{8,1,1}$ WG mode using a 30 mm diameter cylinder and several different height values. Fig. 10 shows the tuning coefficient as a function of the gap spacing for heights of 5, 7.5, 10, 15, and 20 mm. It is clear that, as the height decreases, the tuning coefficient increases. This can be interpreted as due to an increase in the electromagnetic field density in the gap as the height is decreased. Of course, a limit will eventually be reached when the dimensions can no longer support a mode. Furthermore, as there is more field outside the dielectric, low height systems will exhibit lower quality factors as more energy can be radiated away. However, the transducer can be contained within a superconducting shield to minimize radiative loss. Experiments will still be required to determine how the quality factor behaves as the height is reduced, so that an optimization can be made.

We also examined the tuning coefficients in a cylinder with a diameter of 50 mm. In this case the tuning coefficients at the same heights were lower in the 50 mm system. This is due to the higher field confinement in the sapphire dielectric. To maximize the tuning coefficient, the diameter and height must be minimized while retaining high electrical quality factors.

In summary we observed an exponential increase in tuning coefficient with decreasing height. The rate of increase also was greater as the diameter was reduced. Smaller diameter cylinders also show good tuning coefficients at higher gap spacings, which is an advantage if the gap spacing needs to be large for practical reasons.

V. Transducer Sensitivity

Two major components of noise contribute to the spectral sensitivity of a parametric transducer. The first is due to the pump oscillator phase noise, the spectral sensitivity in m^2/Hz is given by;

$$S_x(f) = \left(\frac{df}{dx}\right)^{-2} S_\phi(f) f^2. \tag{21}$$

Thus, by only increasing the tuning coefficient, df/dx, or by reducing the phase noise of the pump oscillator, $S_\phi(f)$, can improve the sensitivity of this component. The second component of noise is due to the noise temperature of the microwave amplifier in the readout system.

The re-entrant cavity motion transducer currently used as the readout of the resonant-bar gravitational wave antenna at UWA, possesses a displacement sensitivity of 3×10^{-17} m/$\sqrt{\text{Hz}}$, which is limited by the readout microwave amplifier in the demodulation chain after the transducer. The power in the signal sidebands is proportional to $P_{\text{inc}} Q_e^2 (df/dx)^2$ or the electro-mechanical coupling, β_o, shown in (22), where the electromechanical coupling is defined as the ratio of electrical energy in the modulation sidebands to mechanical energy in the acoustic res-

TABLE I
COMPARING THE RE-ENTRANT CAVITY TRANSDUCER WITH THE CRYOGENIC SAPPHIRE TRANSDUCER. THE REMAINING PARAMETERS ARE BASED UPON THOSE OF THE RESONANT-BAR GRAVITATIONAL WAVE DETECTOR AT UWA, WHERE $m = 0.5$ KG, $\omega_m = 2\pi \times 700\ \mathrm{s}^{-1}$. THE ELECTRICAL RESONANT FREQUENCY WAS CHOSEN TO BE 9.0 GHZ IN BOTH CASES.

Parameter	Re-entrant cavity	Sapphire transducer
df/dx (MHz/μm)	300	3
Q_e	10^5	10^8
P_{inc}	50 μW	10 mW
β_e	0.3	1
β_o	3.7×10^{-3}	0.67

onance. This means that the level of displacement noise due to the readout system effective noise temperature is proportional to the inverse of this quantity. Here we show that two orders of magnitude improvement in this noise component can be obtained by using a cryogenic sapphire transducer. The increase arises from the higher electrical Q and incident power that can be achieved in the sapphire transducer, resulting in a higher electromechanical coupling, β_o. In general the factor $P_{\mathrm{inc}}Q_e^2(df/dx)^2$ can be a few orders larger in the sapphire transducer. The factors contributing to the improvement are summarized in Table I.

$$\beta_o = \frac{16P_{\mathrm{inc}}\beta_e}{\omega_o m\omega_m^2(1+\beta_e)}\left(\frac{1}{1+4Q_e^2\omega_m^2/\omega_o^2}\right)^2\left(\frac{Q_e}{f_o}\frac{df}{dx}\right)^2 \quad (22)$$

These results suggest that potential exists for improving the electromechanical coupling using a sapphire transducer. Details on how to relate this to an improvement in sensitivity can be found in [20], [21]. However, if one can increase df/dx, both noise components as discussed may be reduced. Increasing the electrical quality factor and incident power will only reduce the noise due to the readout.

Because of the large tuning coefficient and low Q-value of the re-entrant cavity with respect to the sapphire transducer, the re-entrant cavity is more dependent on the noise due to the microwave amplifier. In contrast, the low tuning coefficient and high Q-value make the sapphire transducer depend mainly on the phase noise of the pump. Thus, any improvement in pump oscillator performance will directly improve the performance of the sapphire transducer but will not improve the re-entrant cavity transducer sensitivity.

A. Microwave Readout Circuit

The microwave read-out circuit used to measure the displacement sensitivity is shown in Fig. 11. The state of the transducer was observed via the phase bridge in the readout circuit. Phase sensitivity was selected by the appropriate adjustment of the phase shifter before the *LO* port of the mixer. The static frequency to voltage conversion ratio

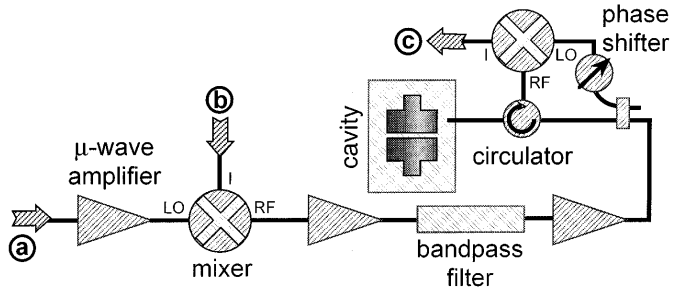

Fig. 11. The microwave read-out circuit used to measure the displacement sensitivity of the transducer. (a) The low phase noise liquid nitrogen cooled (77 K) oscillator signal at a frequency of 8.949 GHz. (b) The HP8662A signal used to tune the frequency source between 7.5 GHz and 10.1 GHz. (c) The output signal from the mixer, which carries the information about the transducers state. The $TM_{8,1,1}$ mode at 10.04 GHz was used for the displacement sensitivity measurements.

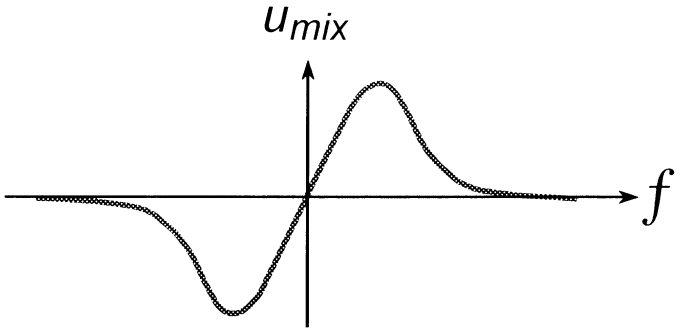

Fig. 12. The static frequency discriminator conversion ratio, $\frac{dV}{df}\Big|_{DC}$, is equivalent to the slope in the linear region. This plot is produced by slowly sweeping across the resonance using a phase sensitive readout.

was measured (as in Fig. 12), and the output voltage was analyzed on an HP35665A spectrum analyzer.

The output voltage was transformed into a displacement by applying the following formula:

$$\delta x_{\mathrm{rms}} = \delta v_{\mathrm{rms}}\left(\frac{df}{dx}\frac{dV}{df}(f)\right)^{-1} \quad (23)$$

where δv_{rms} is the measured rms voltage, df/dx is the tuning coefficient, $\frac{dV}{df}(f)$ is the frequency discriminator conversion ratio (see Fig. 12), f is the offset frequency, and Δf is the full bandwidth of the electrical resonance. The frequency dependent conversion ratio can be expressed as:

$$\frac{dV}{df}(f) = \frac{1}{\sqrt{1+4f^2/\Delta f^2}} \times \left.\frac{dV}{df}\right|_{DC} \quad (24)$$

where the term in the brackets is a filtering factor associated with the transducer's high-Q and small bandwidth. For small offset frequencies relative to the electrical bandwidth, this term converges to unity, and the frequency dependence vanishes. For large offset frequencies, the sensitivity of the frequency discriminator decreases.

The voltage spectra also can be related to oscillator

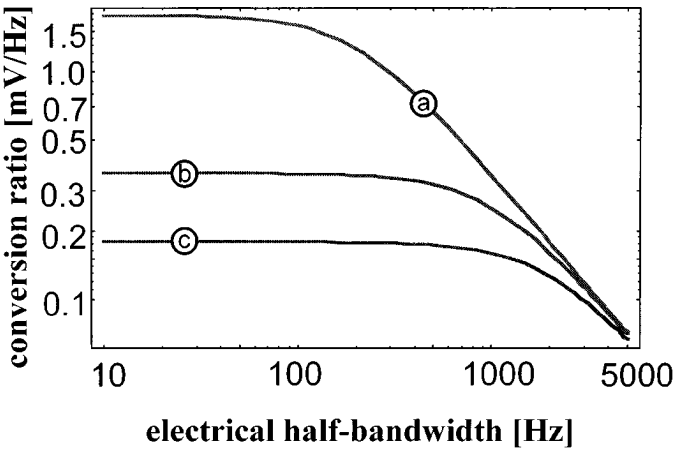

Fig. 13. The frequency discriminator conversion ratio, dV/df, as a function of electrical half-bandwidth. Curve (a) shows the conversion ratio at an offset frequency of 100 Hz, curve (b) at 500 Hz, and curve (c) at 1 kHz. In this plot, $H = 10$ V/$\sqrt{\text{W}}$, $P_{\text{inc}} = 5$ mW, and $\beta_e = 1$.

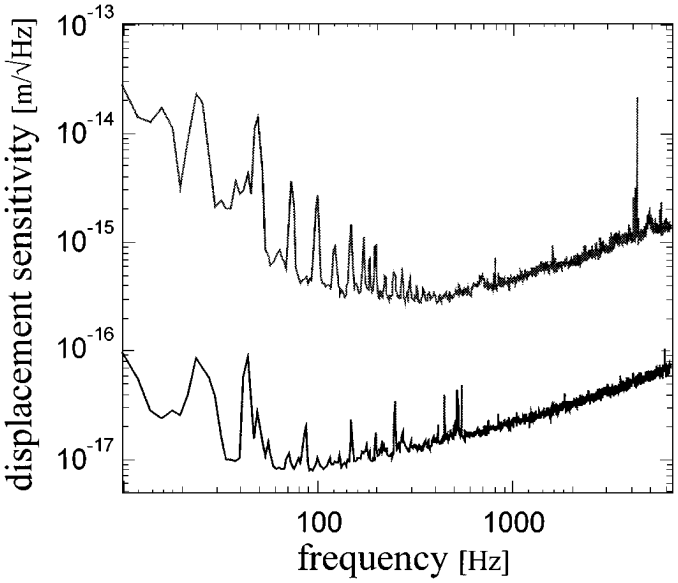

Fig. 14. The upper curve shows the experimental displacement sensitivity of the cryogenic sapphire transducer. At 1 kHz offset, the displacement noise floor was $\delta x_{\text{rms}} \approx 3 \times 10^{-16}$ m/$\sqrt{\text{Hz}}$. The limited displacement sensitivity was attributed to a slightly lower tuning coefficient than could be obtained optimally and a higher than quoted level of pump signal phase noise originating from the HP8662A frequency synthesizer. The low frequency peaks are due to residual mechanical vibrations in the transducer. The lower curve shows the read-out limited noise floor.

phase noise by applying:

$$S_\phi(f) = \delta v_{\text{rms}}^2 \times \left(f \frac{dV}{df}(f) \right)^{-2}. \tag{25}$$

The conversion ratio also can be expressed in terms of the parameters of the frequency discriminator:

$$\left.\frac{dV}{df}\right|_{DC} = H\sqrt{P_{\text{inc}}} \frac{4\beta_e}{1+\beta_e^2} \frac{1}{\Delta f} \tag{26}$$

where H is the power to voltage coefficient of the mixer in units Volts/$\sqrt{\text{Watt}}$, P_{inc} is the power incident upon the cavity, and β_e is the electrical coupling.

The frequency dependent conversion ratio (24) was plotted as a function of electrical half-bandwidth for different offset frequencies as in Fig. 13. This suggests that, to achieve the maximum displacement sensitivity, it is important to operate with an electrical bandwidth of less than the offset frequency of interest. If the bandwidth is greater than the frequency of interest, the effective conversion ratio is smaller because the static conversion ratio decreases as the bandwidth increases. Unfortunately the filtering factor in (24) reduces the sensitivity at high offset frequencies. It has been shown that the optimum bandwidth of the transducer should be of the same order as the frequency of interest [21].

B. Experimental Results

Fig. 14 shows the measured displacement noise floor for the transducer. The optimum displacement sensitivity was $\delta x_{\text{rms}} \approx 2 \times 10^{-16}$ m/$\sqrt{\text{Hz}}$ at 400 Hz offset. The large displacements below 30 Hz are due to seismic and other laboratory noise exciting the normal modes of the vibration isolation. The displacement sensitivity of the transducer decreases as the frequency increases because the discriminator conversion ratio, dV/df, is filtered by the bandwidth of the electrical resonance.

Fig. 15 shows the equivalent phase noise spectra, obtained by applying (25) to the measured voltage spectra. This was equivalent to independent measurements of our pump oscillators phase noise and was due to the phase noise in the HP8662A synthesizer.

The development of the next generation of ultra-low phase noise microwave oscillators at UWA [14], [15] can be expected to increase the displacement sensitivity of the sapphire transducer by several orders of magnitude. The achievable displacement sensitivities are summarized in Fig. 16. Curve (A) shows the sensitivity if a liquid nitrogen cooled sapphire oscillator with a phase noise of -165 dBc/Hz at 1 kHz is used to drive the existing transducer [14]. Curve (B) shows the possible performance if a new low noise oscillator with carrier suppression phase noise cancellation is implemented [15].

VI. Conclusions

A highly sensitive double disk sapphire dielectric transducer that senses the motion with respect to the two disks was developed. An electromagnetic model that predicts the resonant frequency and tuning coefficient of the dielectric system was developed and verified by experiment. We found that the optimum mode was the TM_{711} mode for a resonator of 3 cm in diameter. Also, we determined that the tuning coefficient was maximized by choosing an aspect ratio that has a large diameter with respect to the height. By implementing a microwave pump oscillator of

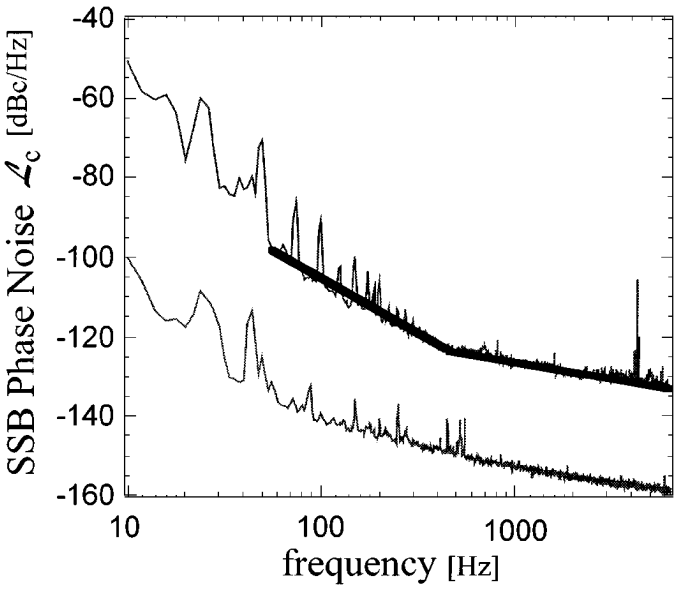

Fig. 15. The upper curve shows the equivalent single side band (SSB) phase noise spectra obtained using the same data as shown in Fig. 14. At 1 kHz offset the phase noise was $L_c \approx -128$ dBc/Hz. This was greater than 10 dBc/Hz worse than expected from the composite tunable low phase noise pump signal. The lower curve represents the read-out limited noise floor.

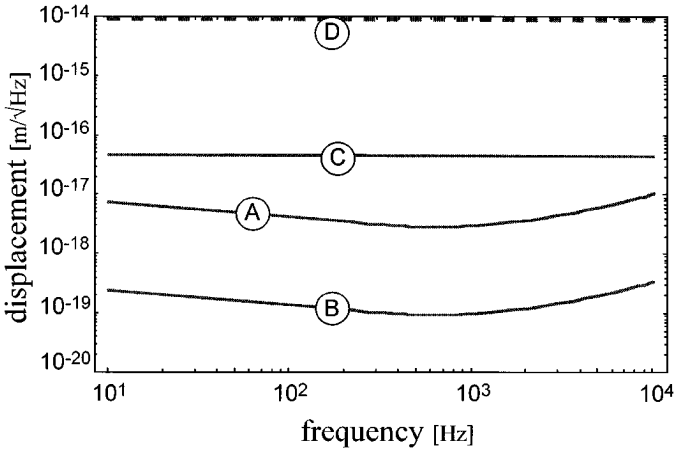

Fig. 16. The projected displacement sensitivity of the transducer using the improved phase noise sources. Curve A shows the expected sensitivity using a liquid nitrogen cooled sapphire oscillator with phase noise of −165 dBc/Hz at 1 kHz [14]. Curve B shows the displacement sensitivity if the proposed 20 dBc/Hz improvement can be made to the liquid nitrogen cooled sapphire oscillator [15]. Curve C shows the best displacement sensitivity achieved for a superconducting re-entrant cavity transducer [6], which is about the same as an inductive SQUID transducer [7]. Curve D shows the estimated displacement sensitivity of a piezoelectric transducer used by the first room temperature gravitational wave detectors.

SSB phase noise −125 dBc/Hz at 1 kHz offset, the sensitivity with respect to displacement was measured to be of the order 10^{-16} m/$\sqrt{\text{Hz}}$. We have shown that this can be improved with existing technology to 10^{-18} m/$\sqrt{\text{Hz}}$, and that, in the near future, this may be further improved to 10^{-19} m/$\sqrt{\text{Hz}}$.

Acknowledgments

The authors would like to thank the members of the UWA Gravitational Wave, Precision Oscillators and Quantum Measurement research groups for their assistance and enthusiasm.

References

[1] V. B. Braginsky, V. I. Panov, and V. D. Popel'nyuk, *JETP Lett.*, vol. 33, p. 405–407, 1981.

[2] W. C. Oelfke and W. O. Hamilton, "Design and preparation of a high-Q niobium re-entrant cavities for physical measurements," *Rev. Sci. Instrum.*, vol. 54, pp. 410–414, 1983.

[3] K. Tsubono, M. Okashi, and H. Hirakawa, "Parametric transducer for gravitational radiation detector," *Jpn. J. Appl. Phys.*, vol. 25, pp. 622–626, 1986.

[4] M. F. Bocko, W. W. Johnson, and V. Iafolla, "A rf superconducting electromechanical transducer for gravitational wave antennas," *IEEE Trans. Magn.*, vol. 25, p. 1358–1362, 1989.

[5] P. J. Veitch, "Parametric transducers," in *The Detection of Gravitational Waves*, D. G. Blair, Ed. Cambridge: Cambridge Univ. Press, 1991, pp. 186–225.

[6] D. G. Blair, E. N. Ivanov, M. E. Tobar, P. J. Turner, F. V. Kann, and I. S. Heng, "High sensitivity gravitational wave antenna with parametric transducer readout," *Phys. Rev. Lett.*, vol. 74, pp. 1908–1911, 1995.

[7] N. D. Solomonson, W. O. Hamilton, W. W. Johnson, and B. Xu, "Construction and performance of a low noise inductive transducer for the Louisiana State University gravitational wave detector," *Rev. Sci. Instrum.*, vol. 65, p. 174–180, 1994.

[8] V. B. Braginsky and F. Y. Khalili, *Quantum Measurement*. Cambridge: Cambridge Univ. Press, 1992.

[9] M. E. Tobar, E. N. Ivanov, D. K. L. Oi, B. D. Cuthbertson, and D. G. Blair, "Sapphire test-masses for measuring the standard quantum limit and achieving quantum nondemolition," *Appl. Phys. B*, vol. 64, pp. 153–166, 1997.

[10] H. Peng, D. G. Blair, and E. N. Ivanov, "An ultra high sensitivity transducer for vibration measurement," *J. Phys. D, Appl. Phys.*, vol. 27, p. 1150–1155, 1994.

[11] I. A. Bilenko, E. N. Ivanov, M. E. Tobar, and D. G. Blair, "Sapphire high-Q low temperature transducer for resonant bar gravitational wave antennas," *Phys. Lett. A*, vol. 211, pp. 139–142, 1996.

[12] B. D. Cuthbertson, M. E. Tobar, E. N. Ivanov, and D. G. Blair, "Parametric back action effects in a high-Q cryogenic sapphire transducer," *Rev. Sci. Instrum.*, vol. 67, pp. 2435–2442, 1996.

[13] G. J. Dick, D. G. Santiago, and R. T. Wang, "Temperature-compensated sapphire resonator for ultra-stable oscillator capability at temperature above 77K," *IEEE Trans. Ultrason., Ferroelect., Freq. Contr.*, vol. 42, pp. 815–819, 1995.

[14] R. A. Woode, M. E. Tobar, E. N. Ivanov, and D. G. Blair, "An ultra-low noise microwave oscillator based on a high-Q liquid nitrogen cooled sapphire resonator," *IEEE Trans. Ultrason., Ferroelect., Freq. Contr.*, vol. 43, pp. 936–941, 1996.

[15] E. N. Ivanov, M. E. Tobar, and R. A. Woode, "Ultra-low noise microwave oscillator with advanced phase noise suppression system," *IEEE Microwave Guided Wave Lett.*, vol. 6, no. 9, pp. 312–314, 1996.

[16] M. E. Tobar and A. G. Mann, "Resonant frequencies of higher order modes in cylindrical anisotropic dielectric resonators," *IEEE Trans. Microwave Theory Tech.*, vol. 39, pp. 2077–2083, 1991.

[17] H. Peng, "A Sapphire dielectric resonator transducer," in *Department of Physics*. Ph.D. Thesis, Perth: The University of Western Australia, 1995.
[18] D. Kajfez and P. Guillon, *Dielectric Resonators*. Norwood MA: Artech House, 1986.
[19] M. E. Tobar, "Gravitational wave detection and low noise sapphire oscillators," in *Department of Physics*. Ph.D. Thesis, Perth: The University of Western Australia, 1993.
[20] M. E. Tobar and D. G. Blair, "Parametric transducers for resonant bar gravitational wave antennas," *J. Phys. D, Appl. Phys.*, vol. 26, pp. 2276–2291, 1993.
[21] M. E. Tobar and D. G. Blair, "Sensitivity analysis of a resonant-mass gravitational wave antenna with a parametric transducer," *Rev. Sci. Instrum.*, vol. 66, pp. 108–110, 1995.

Brett D. Cuthbertson was born in Perth, Western Australia, on July 12, 1973. He received the B.Sc. (Honours) degree in physics at the University of Western Australia, Perth.

From 1994 to July 1995 he undertook a Master's degree in the Department of Physics at the University of Western Australia, where he investigated the cryogenic sapphire transducer. He then moved to the national capital to commence a Ph.D. in the Department of Physics and Theoretical Physics at the Australian National University in Canberra.

His research now involves the trapping and cooling of atoms to develop practical "Atom Optical" components. His research interests are wide and varied, but currently flow around the development of an atom optical beam splitter and the construction of an experiment to produce a Bose-Einstein Condensate. He also delights in the preparation of fine food to be consumed with an accompanying fine wine, and would like to spend more time exploring, photographing, and protecting the natural beauty of Australia. He firmly believes the market-oriented western world has lost the plot, and its idealogy needs to be reconsidered. Needless to say, he also has an inquiring interest in global economics.

Michael E. Tobar (S'87–M'88–S'89–A'90–S'91–A'92–M'96) was born in Maffra, Australia, on January 3, 1964. He received the B.Sc. degree in theoretical physics and mathematics in 1985, and the B.E. (honors) degree in electrical and computer systems engineering in 1988, both from Monash University, Melbourne, Australia.

From 1989 to 1992 he was a Ph.D. student in the Department of Physics, University of Western Australia, Perth, and from 1992 to 1993 he was appointed a research associate. His dissertation was entitled, "Gravitational wave detection and low noise sapphire oscillators."

From 1994 to 1996 he was awarded an ARC Australian Postdoctoral Research Fellowship at the University of Western Australia, and during 1997 he was appointed a senior research associate. In 1997–1998, he was awarded a JSPS Fellowship at the University of Tokyo. For his research achievements, he was awarded the 1997 Australian Telecommunications and Electronics Research Board (ATERB) medal, a 1996 URSI young scientist award, and is co-winner of the 1994 Japan Microwave Prize. His research interests include low-noise oscillators, measurement systems and components, ultrasensitive transducers, carrier suppression techniques, quantum measurement, gravitational wave detection, cryogenic systems, electromagnetics, microwaves, optics, interferometric systems, and mathematical modeling.

Eugene N. Ivanov was born in Moscow on August 14, 1956. He received the Ph.D. degree in radio electronics from Moscow Power Engineering Institute in 1987. From 1980 to 1990, he was involved in the design of low-noise Gunn diode oscillators and analysis of electromagnetic dielectric resonators with whispering gallery modes.

In 1991, Dr. Ivanov joined the Gravitational Research Laboratory at the University of Western Australia. In 1993 he developed a microwave read-out system for the resonant mass gravitational wave detector. In 1995 he suggested a new frequency stabilization technique that resulted in 25 dB improvement in the phase noise performance of X-band oscillators. In 1996 he designed a microwave interferometric noise measurement system with sensitivity approaching the thermal noise limit. The extremely low noise floor of such a system is close to −193 dBc/Hz at 1 kHz Fourier frequency allowed the first experimental evidence of intrinsic l/f noise in microwave isolators.

Dr. Ivanov is a co-winner of 1994 Japan Microwave Prize.

David G. Blair is an associate professor at the University of Western Australia. He is Director of The Australian International Gravitational Research Centre. His work focuses on technology development for gravitational wave astronomy, including ultrastable optical and microwave oscillators, as well as the operation and analysis of data from gravitational wave detectors.

He won the 1995 Australian Institute of Physics Boas Medal for Research Achievements in the last 5 years.